IN-46-CR
77034
P-24

CRUSTAL DEFORMATION ALONG THE SAN ANDREAS, CALIFORNIA

Final Technical Report
Period: February 1, 1991 - January 31, 1992

Grant No. NAG 5-1398
Grant Recipient: University of Michigan, Ann Arbor
Principal Investigator: Professor Victor C. Li
NASA Technical Officer: Dr. Herbert Frey, Investigations Manager
Government Grants Officer: Gloria R. Blanchard

Effective Date of Grant: Feb. 1, 1991
Effective Expiration Date: Jan. 31, 1992
Amount of Grant: $55,650

Submitted Date: March, 2, 1992
Sponsored by the

Crustal Dynamics Program
National Aeronautics and Space Administration

Victor C. Li (P.I.)
2326, G.G. Brown Building,
Department of Civil and Environmental Engineering,
University of Michigan, Ann Arbor,
MI 48109-2125
(313)764-2399

INTRODUCTION

This is a final technical report of the project entitled "Crustal Deformation Along the San Andreas, California" supported by NASA Crustal Dynamics Program, for the period Feb. 1, 1991 - Jan. 31, 1992, based on funding from the Grant No. NAG 5-1398 awarded to the University of Michigan, Ann Arbor.

The goal of this project is to achieve a better understanding of the regional and local deformation and crustal straining processes in western North America, particularly the effect of the San Andreas and nearby faults on the spatial and temporal crustal deformation behavior. Construction of theoretical models based on the mechanics of coupled elastic plate /viscoelastic foundation and large-scale crack mechanics provide a rational basis for the interpretation of seismic and aseismic anomalies and expedite efforts in forecasting the stability of plate boundary deformations.

In the present period, special focus is placed on the three dimensional time-dependent surface deformation due to localized slippage in a elastic layer coupled to a visco-elastic substrate. The numerical treatment of this problem is based on a 3-D boundary element technique derived in previous periods of research for elastic layered media. Extension to visco-elastic coupling demands the derivation of 3-D time-dependent Green's function. This has been

successfully achieved. This method has been applied to analyze the viscoelastic surface displacements due to a dislocated embedded patch. Surface uplift as a function of time and position are obtained. Comparisons between surface uplift for long and short dislocated patches are made.

SUMMARY OF PROJECT ACHIEVEMENTS TODATE

Major achievements for the duration of the project are summarized below:

1. Developed and completed a model of coupling between the elastic lithosphere and viscoelastic asthenosphere which incorporate the sub-mantle steady state motion as a long term driving force, and the transient loading and reloading of the plate boundary in earthquake cycles. This model suggests significant non-linearity in the stress-accumulation process over an earthquake cycle at a plate boundary.

2. Developed and completed the modeling of crustal deformation (referred to as the Li-Rice model hereon) which varies with time and space at a strike-slip plate boundary embedded in the plate structure described in (1) above.

3. From (1) and (2), and whole cycle San Andreas composite geodetic data, the surface elastic plate thickness is constrained to 20-30 km, and the viscoelastic relaxation time is constrained to 10-16 yr.

4. The predicted surface velocity profiles are in good agreement with geodetic measurements at several locations along the San Andreas where such data is available. Locations studied include Point Reyes area and the Palmdale area. Predicted surface velocity profile at Palmdale area agree with the recently obtained field data. Note that model prediction is made independently of the geodetic field data indicated.

5. Development of a model similar to the Li-Rice model for complex plate boundaries, including plate boundaries exhibiting surface fault creep, and plate boundaries with sub-parallel faults. Application of this model to the Parkfield area in Central California and to the Coachella-Valley area in Southern California is

performed. The predicted surface velocity for the Coachella-Valley area can be fitted to recent VLBI and ground based geodetic data.

6. Comparison of the single line dislocation model of Savage and Burford with the Li-Rice model reveals that the locked depth and deep aseismic slip rate are significantly overestimated for the single line dislocation model using geodetic data as constraining information. Further, over the span of an earthquake cycle, the single line dislocation model is shown to predict a shallower locked depth and a larger deep slip rate for a velocity profile associated with a time earlier in an earthquake cycle in comparison to that associated with a time later in an earthquake cycle. This is physically implausible. The suggestion from this analysis is that while the Savage/Burford single line-dislocation model is simple to use and understand, it also imposes severe limitation in direct physical interpretation of fault locked depth and deep aseismic slip rate, as well as other tectonic implications.

Since the last technical report, our work has focused on the study of three dimensional effect of localized slippage in a elastic layer coupled to a visco-elastic substrate. This method has been applied to analyze the viscoelastic surface displacements due to a dislocated embedded patch. Surface uplift as a function of time and position are obtained. Comparisons between surface uplift for long and short dislocated patches are made.

INVESTIGATION ON 3-D TIME DEPENDENT VISCOELASTIC RESPONSE

The viscoelastic Green's functions considered were the displacement and stress fields due to a nucleus of strain located in an elastic plate ($0 \le z \le H$) with a free surface at $z=0$ and a perfectly bonded lower (Figure. 1) viscoelastic halfspace at $z \ge H$. These Greens' functions will be used in surface integrals over slip patches of any arbitrary shapes, and can be used to deduce crustal deformations over a range of time after the patch slippage.

The viscoelastic model used for the lower halfspace is that of a Maxwell fluid described by

$$\frac{1}{2\mu}\dot{s}_{ij} + \frac{1}{\eta_s}s_{ij} = \dot{e}_{ij} \tag{1}$$

$$\frac{1}{2K}\dot{\sigma}_{kk} + \frac{1}{\eta_d}\sigma_{kk} = \dot{\varepsilon}_{kk} \tag{2}$$

where s_{ij} and e_{ij} are the deviatoric part of the stress and strain components σ_{ij} and ε_{ij}. A dot over a variable indicates rate with respect to time, μ and K are the shear and bulk modulus, and η_s and η_d are the shearing and volumetric viscosities respectively. For a quasi-static problem where the inertial terms are negligible, the only time dependence occurs in the boundary conditions and constitutive relations. It can be shown that the constitutive relations is similar in form in the Laplace transformed space to the elastic stress-strain relations in real space, but with the shear and bulk moduli replaced by moduli dependent on the Laplace variable "s". Thus the correspondence principle can be applied to solve the viscoelastic problem (Christensen, 1982).

Within the context of the image method developed by us (Fares and Li, 1988), and for the case when the nucleus of strain lies in the plate, field variables are only required in the plate, and where only the lower halfspace is viscoelastic, the only instances where moduli in Laplace transformed space which are dependent on the Laplace variable are in the "reflection" operators. It can be shown that there are in general four characteristic time scales for the response of a point source located in a plate perfectly bonded to one Maxwellian halfspace. The Laplace transform of a suddenly applied and then maintained unit excitation is 1/s. These considerations lead to insights into the behavior of the viscoelastic solutions. Specifically, the Laplace inverse of the terms in the solution after the correspondence principle is applied :

$$L^{-1}\left[\frac{1}{s}\frac{\bar{A}^-}{A^-}\right] = \left(1 - \frac{c}{\Omega_A}\right) + e^{-\Omega_A t} \tag{3}$$

$$L^{-1}\left[\frac{1}{s}\frac{\bar{B}^-}{B^-}\right] = \left(1 - \frac{d}{\Omega_{B1}} + \frac{e}{\Omega_{B2}}\right) + \frac{d}{\Omega_{B1}}e^{-\Omega_{B1}t} - \frac{e}{\Omega_{B2}}e^{-\Omega_{B2}t} \tag{4}$$

$$L^{-1}\left[\frac{1}{s}\frac{1-\bar{\gamma}}{1+\bar{\gamma}}\right]=\left(p+\frac{q}{\Omega}\right)+\frac{q}{\Omega}e^{-\Omega t} \qquad (5)$$

where the lower case letter variables and Ω are defined in terms of the moduli. Other terms are defined in Fares and Li (1988). After some algebra, the terms that are not multiplying the exponential functions in (3) - (5) can be simplified to the following

$$1-\frac{c}{\Omega_A}=-\frac{1}{\delta}\frac{1}{A^-} \qquad (6)$$

$$1-\frac{d}{\Omega_{B1}}+\frac{e}{\Omega_{B2}}=-\delta\frac{1}{B^-} \qquad (7)$$

$$p+\frac{q}{\Omega}=1 \qquad (8)$$

Therefore, the short time response of (3) - (5) (i.e. t -> 0+) corresponds to the halfspace being purely elastic and the long time response (from (6)-(8)) corresponds to a stress free boundary condition on the lower interface.

The following observations are noted: i) The effective time scale of $t^m e^{-\lambda t}$ is longer than the effective time scale of $t^n e^{-\lambda t}$ when m>n, ii) the components of the product of the reflection matrices for "farther off" images contain polynomials in "t" with higher degrees multiplying the exponential terms, and iii) the relative contribution of "farther off" images increases as we get farther from the source location in the plate for fixed values of moduli. Thus the effective relaxation rate decreases as the distance from the source region increases. This concept could be associated with the stress diffusion phenomenon.

As a numerical example of the above remarks, figures 2 and 3 show the surface displacement components u_x and u_z respectively for embedded nuclei of strain (or moment sources) located at x=y=0 and z=0.5H and having the normal vector $\underline{n}$ = (0,1,0) and (1,0,0) respectively and Displacement Discontinuity (DD) components $\Delta\underline{u}$ = (1/μA).(1,0,0) and (1/μA).(0,0,1) respectively, where μ is the shear modulus and "A" is an "effective area". The surface displacements are

plotted for y=z=0 and 0≤/H≤4.0; the surface displacements are antisymmetric with respect to reflection of the x-axis. The time "t" at which the curves are plotted are ωt = 0.0, 0.5, 1.0, 2.0, 3.0, 4.0, 5.0, 10.0, 15.0 and 30.0 for figure 2 and ωt = 0.0, 1.0, 3.0, 5.0, 7.0, 10.0, 12.5 and 30.0 for figure 3; for both figures, the level of displacement increases with time (at least) in the range of 0≤x/H≤1.0.

The "diffusion" aspect of the displacement fields can be recognized with the help of the following observations. In figure 2, consider two separate locations, one relatively "close" to the source (e.g. at x/H=0.5) and one relatively "far" from the source (e.g. at x/H=4.0). While the displacement seems to increase most at "early" times afterwhich this increase "slows down" for the closer location, the displacement increases relatively "faster" at "later" times for the "farther" location. The above remarks can be interpreted as being due to a "disturbance" which reaches and "saturates" the displacement field closer to the source and "diffuses" to reach farther off points from the source at "later" times. The time increments at which curves are plotted in figure 2 are not equal. Specifically, the last time step ωt = 30.0 is chosen so that no significant change in the displacement magnitudes (for all locations 0≤x/H≤4.0) is noticed beyond that time step. The diffusion aspect in figure 3 is more readily apparent. A "disturbance" in the displacement magnitudes "seems" to be "penetrating" (or diffusing) farther from the source with increase in time. Again (for clarity of the figures), the time increments at which curves are plotted in figure 3 are not equal and ωt = 30.0 is chosen so that no significant change in the displacement magnitudes (for all location 0≤x/H≤4.0) is noticed beyond that time step.

INVESTIGATION OF VISCOELASTIC SURFACE DISPLACEMENTS DUE TO A DISLOCATED EMBEDDED PATCH

A time-dependent model consisting of slippage (or dislocation) along a surface in an elastic plate overlying a viscoelastic foundation is usually used in geophysical applications to study (or to take into account) postseismic surface deformations (i.e. surface deformations that occur "after" an earthquake). Two-dimensional "thrust" slippage and antiplane "strike slip" (both assume infinitely long faults) viscoelastic models have been repeatedly considered by many researchers (e.g. Nur and Mavko 1974, Smith 1974, Savage and Prescott 1978,

Thatcher and Rundle 1979, Lehner et al. 1981, Li and Rice 1987 and Reilinger 1986).

In our research, the surface uplift due to uniform "thrust" slippage that occurs and is maintained along an inclined finite rectangular patch (two different lengths are considered) in a plate has been analyzed. The geometry of the side and top views of those two patches are shown in figure 4. The aim of this study is to present surface deformations due to a 3-D viscoelastic model of a layered earth, and to try and discern (if any) deformation feature differences between a 2-D and a 3-D model. The short patch represents a 3-D model and the long patch represents an approximate 2-D model. The calculation of the time-dependent surface uplift is obtained by the integration of the viscoelastic Green's functions discussed earlier over the surface of the patches using specialized integration techniques.

The geometric parameters of the model are as shown in figure 4 (the short and long patches having lengths of 1.2H and 5H respectively). Unit slippage (i.e. 1H) is prescribed to occur uniformly over the surface of each patch; the surface uplift plots to be presented in this section (being linearly proportional to the amount of slippage along the patch) can be alternately viewed as being normalized by the slippage value. The elastic properties are such that the plate and the halfspace have identical shear modulus "G" and Poisson' ratio "ν"; the shear modulus "G" is taken to be "1" (arbitrary units) and Poisson's ratio "ν" is taken to be 0.25. The units of the shear modulus does not affect the surface deformation values but serves to specify how much "force" has to be applied at the opposing slipping surfaces in order to produce the slippage (in geophysical applications, the shear modulus is said to affect the "moment" and "stress drop" on the patches). The volumetric deformation is purely elastic and the deviatoric deformation is a Maxwell model with a viscosity parameter $\eta = 20$ (arbitrary units); the ratio of "$\eta/(2G)$" determines the characteristic time "t_r" (time units depend on the units of both "η" and "G"). The above values of "η/G" and "ν" imply $\omega = 2G/\eta = 0.1$, $\Omega = 0.5\omega$, $\Omega_A = 0.33w$, $\Omega_{B1} = 0.9\omega$ and $\Omega_{B2} = 0.24\omega$; the preceding values of Ω, Ω_A, Ω_{B1} and Ω_{B2} show that the four distinct exponential time-scales lie within an interval of "$1/\omega$" to "$4.2/\omega$" for a model having the elastic properties of the plate and halfspace equal, and with Poisson's ratio equal to 0.25.

The surface uplift values along the x-axis (z=0, y=0 in figure 4) for $-4.2 \le x/H \le 4.2$ and up till sufficiently long times (so that "steady state" has occurred in the range $-0.7 \le x/H \le 0.7$) are presented in figures 5 to 13 for both the short (figures 5 to 9) and long patch (figure 10) as well as for comparisons between the two patches (figures 11 to 13). A discussion of these results will be next presented.

First consider the uplift values due to the short patch. For convenience the deformation pattern will be divided into three sections. These sections numbered 1 to 3 lie roughly between $-4.2 \le x/H \le 0.6$, $-0.6 \le x/H \le o.04$ and $0.4 \le x/H \le 4.2$ respectively. The material lying at $x/H \le 0.3$ is being "pushed" onto a narrow "gap" between the free surface and the closest edge of the rectangular patch to that free surface. This "squeezing" effect causes a sharp peak in the uplift values to occur in section "2". However, the material lying at $x/H \le 0.3$ is being "anchored" to a halfspace which is steadily relaxing, and hence with time, the uplift values in section "2" move in the direction of "imposed slippage" on the upper surface of the patch. Finally, material is being driven below (or being pushed under) the patch (starting from $x \le 0.3$ to $x \ge -0.3$) and this material is being resisted with a "floor" which is steadily relaxing; hence the uplift values in section "3" move in the direction of "imposed slippage" on the lower surface of the patch. The evolution of uplift with time is quite complex in detail, as can be seen in figures 6-9. Some features that can be discerned in those figures is an exponential decay of surface deformation towards a "steady state" in section "1" (figures 7 and 8), as well as some diffusional behavior which can be deduced from the "more elongated" and "longer lived activity" time behavior of locations that are farther off from the patch (figures 6 and 9); however, from the convergence studies of chapter 2, the numerical accuracy of the surface deformations of "faraway" locations are not very certain, and exact judgment on the results cannot be made. The next discussion will compare the "short" (3-D) versus the "long" (2-D) surface uplifts.

The surface uplift for the "long" patch is shown in figure 10, and is not qualitatively much different from the surface uplift due to the "short" patch. A general observation is that the surface uplift values for the "long" patch has higher peaks and varies more with time than the "short" patch; this observation is

probably due to the higher compliance inherent in a longer patch (by having less "side supports"). Figures 11 to 13 show comparisons at short, intermediate and long time values between the uplift values of the "short" and "long" patch. The higher "inherent compliance" of the longer patch causes the "anchoring" in section "1" (of the plots) to be less effective and the "driving under" in section "3" (of the plots) to be more effective than for the shorter patch.

REFERENCES

Fares, N. and V.C. Li, "General Image Method in a Plane-Layered Elastostatic Medium", J. Applied Mechanics, 55, 4, 781-785, 1988.

Christensen, R.M., "Theory of Viscoelasticity, An Introduction", Second Edition, Academic Press, 1982.

RELATED PUBLICATIONS

Li, V.C., H.S. Lim and S. Cohen, "Near Fault Surface Deformation Based on the Elsasser Model", EOS, Vol. 67, No. 16, 308, 1986.

Li, V.C. and N. Fares, "Rupture Processes in the Presence of Creep Zones", in Earthquake Source Mechanics, (ed. S. Das, J. Boatwright, C. H. Scholz), Maurice Ewing V. 6, pp. 71-80, 1986.

Fares, N. and V. C. Li, "Image method for the derivation of point sources in elastic problems with plane interfaces," Research Report No. R86-01, Dept. of Civil Engineering, MIT, June, 1986.

Li, V.C., "Mechanics of Shear Rupture Applied to Earthquake Zones", in book chapter in Fracture Mechanics of Rock, pp. 351-427, ed. B. Atkinson, Academic Press, 1987.

Fares, N. and V. C. Li, "An Indirect Boundary Element Method for 2-D Finite/Infinite Regions with Multiple Displacement Discontinuities", Journal of Engineering Fracture Mechanics, Vol. 26, No. 1, pp. 127-141, 1987.

Li, V. C. and H. S. Lim, "Lithosphere Basal Traction and Surface Deformation Rates", EOS, Vol 68, No. 16, 415, 1987.

Li, V.C. and J.R. Rice, "Crustal Deformation in Great California Earthquake Cycles", Vol. 92, 11533-11551, J. Geophysical Research, 1987.

Li, V.C., S. Hull and Tianqing Cao, "Postseismic Stress and Pore Pressure Readjustment and Aftershock Distributions", Vol. 143, Tectonophys., 1987.

Li, V.C. and H.S. Lim, "Modelling Surface Deformation at Complex Strike-Slip Plate Boundaries", J. Geophys. Res., Vol. 93, pp. 7943-7954, 1988.

Li, V.C. and H.S. Lim, "The Stress Field in an Edge Cracked Plate in Anti-plane Deformation", Int'l J. of Fracture, 38, 2, pp. 143-155, 1988.

Fares, N. and V.C. Li, "3-D Boundary Element Method for Cracks in a Plate", Int'l J. for Numerical Methods in Engineering, 7, 28, pp. 1703-1713, 1989.

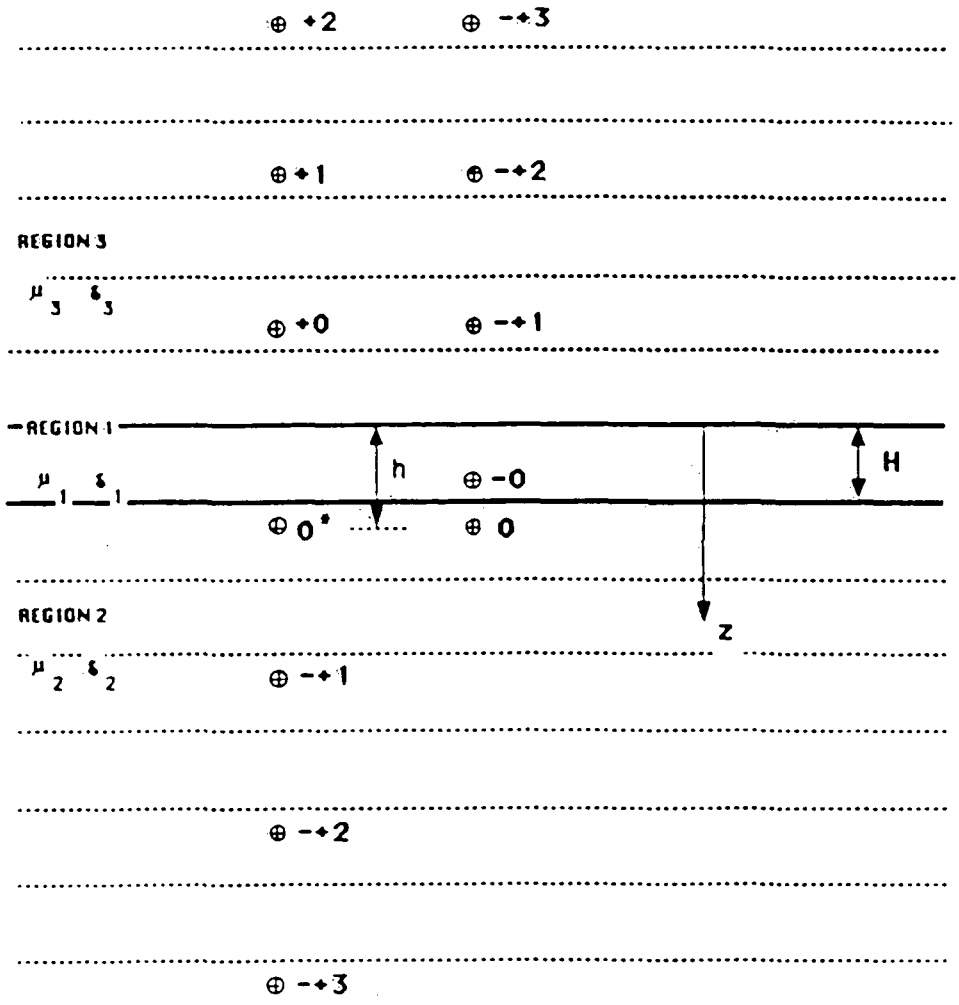

Figure 1

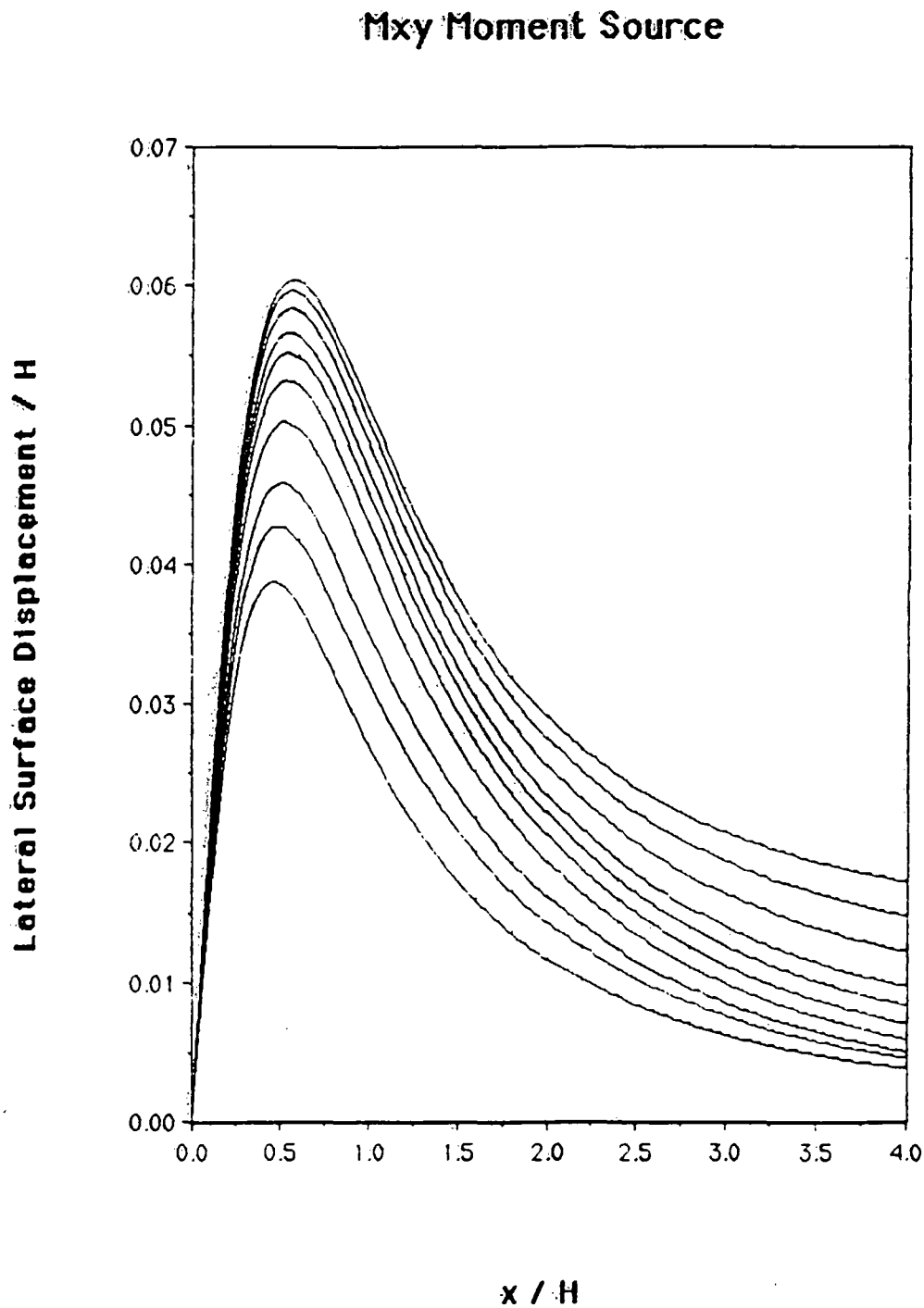
Mxy Moment Source
Lateral Surface Displacement / H
0.07
0.06
0.05
0.04
0.03
0.02
0.01
0.00
0.0
0.5
1.0
1.5
2.0
2.5
3.0
3.5
4.0
x / H

Figure 2

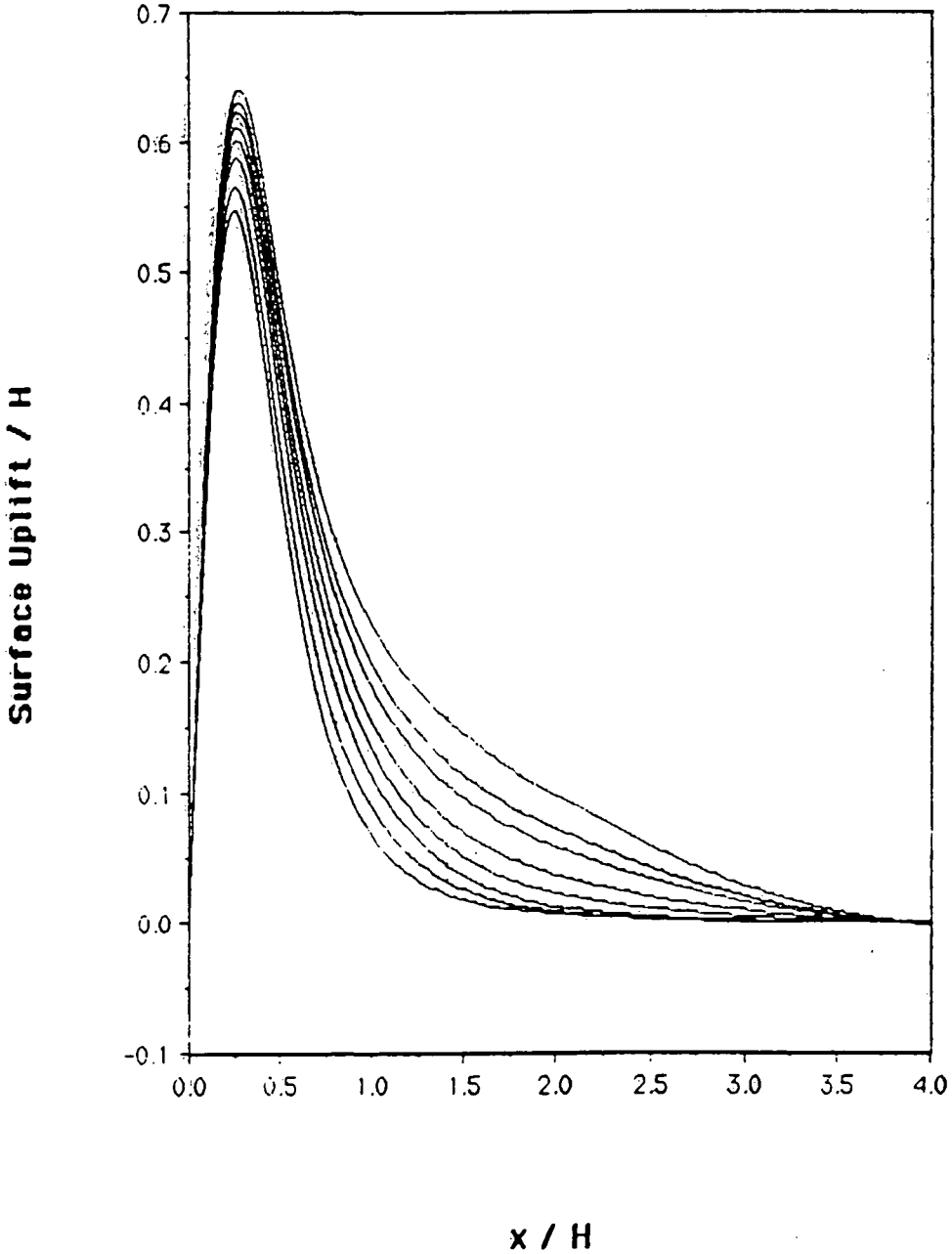
Mxz Moment Source
Surface Uplift / H
0.7
0.6
0.5
0.4
0.3
0.2
0.1
0.0
-0.1
0.0
0.5
1.0
1.5
2.0
2.5
3.0
3.5
4.0
x / H

Figure 3

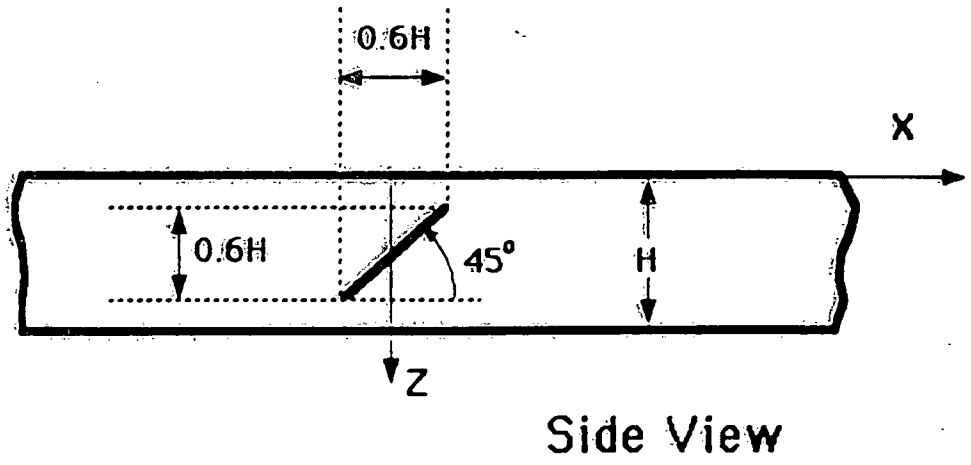

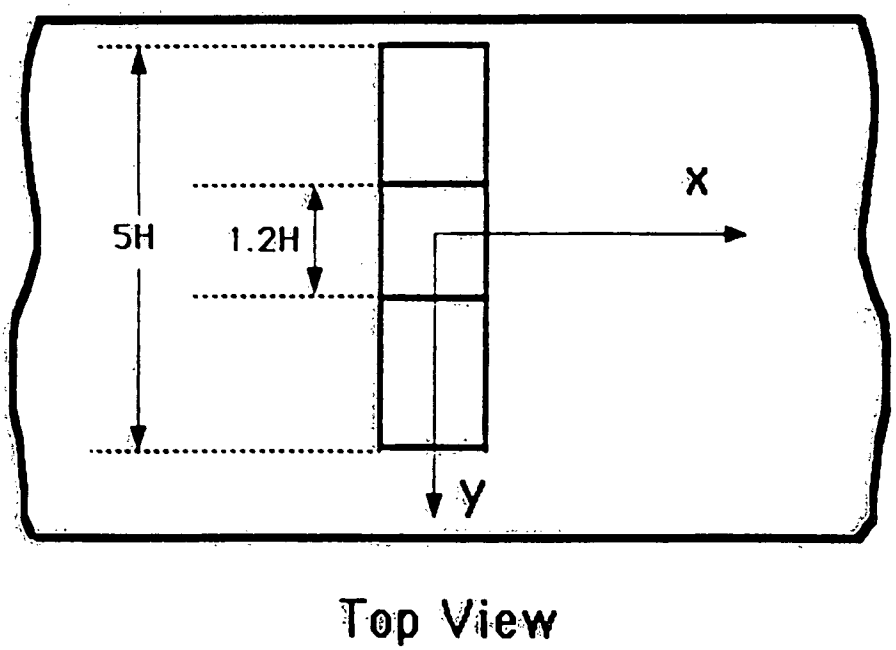

Figure 4

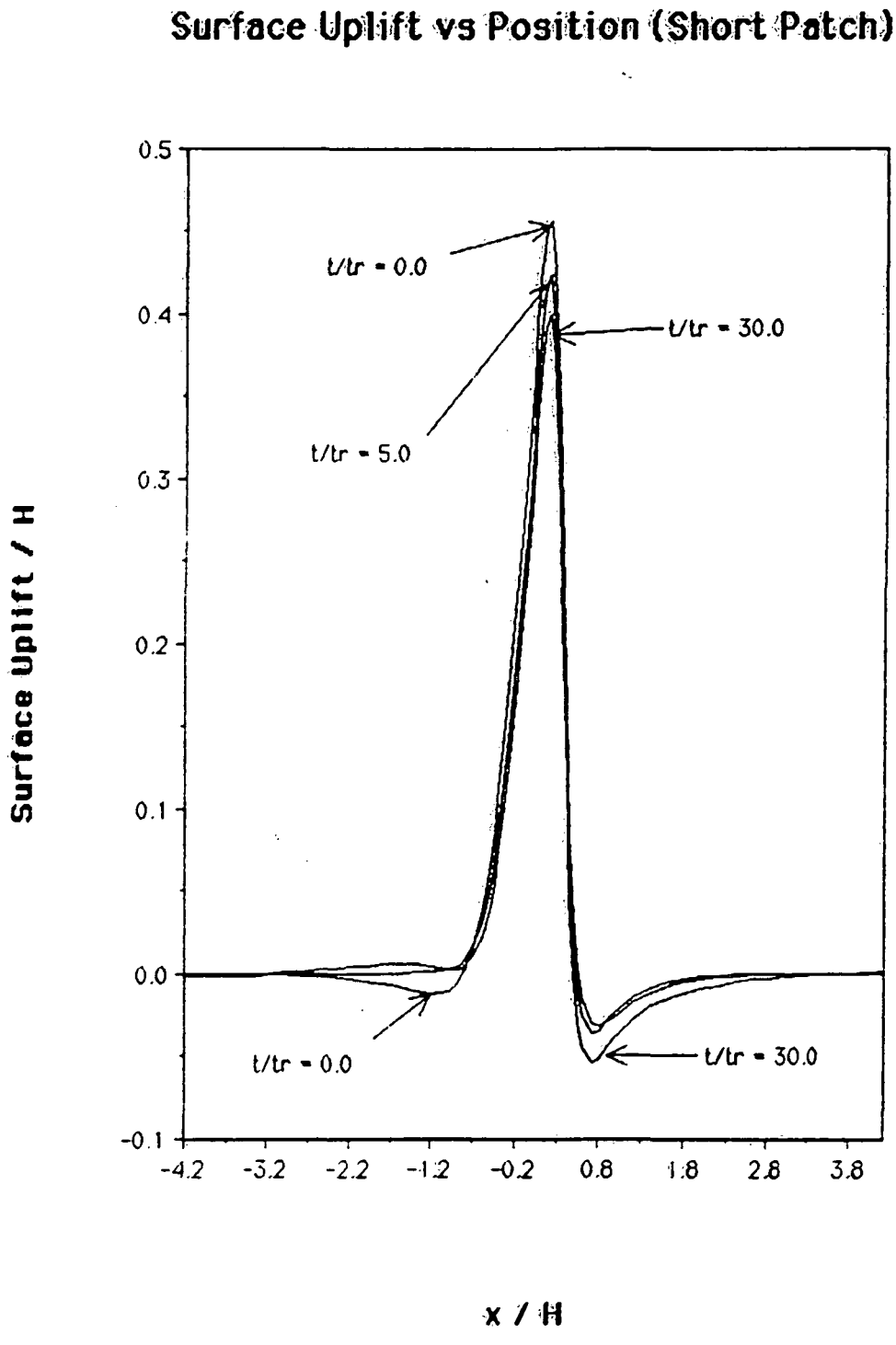
Surface Uplift vs Position (Short Patch)
Surface Uplift / H
0.5
0.4
0.3
0.2
0.1
0.0
-0.1
-4.2
-3.2
-2.2
-1.2
-0.2
0.8
1.8
2.8
3.8
t/tr = 0.0
t/tr = 30.0
t/tr = 5.0
t/tr = 0.0
t/tr = 30.0
x / H

Figure 5

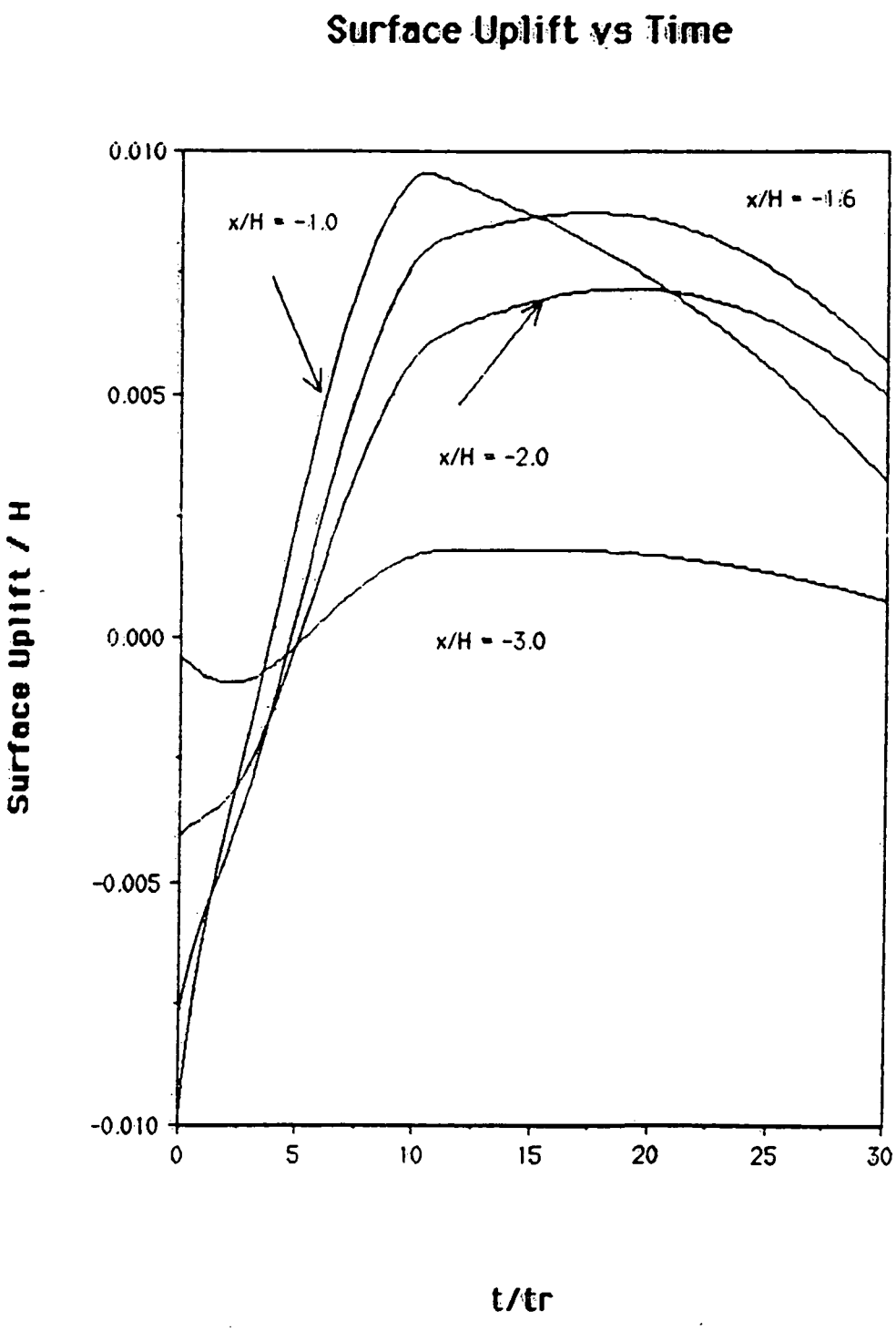
Surface Uplift vs Time
0.010
0.005
0.000
-0.005
-0.010
0
5
10
15
20
25
30
x/H = -1.0
x/H = -1.6
x/H = -2.0
x/H = -3.0
Surface Uplift / H
t/tr

Figure 6

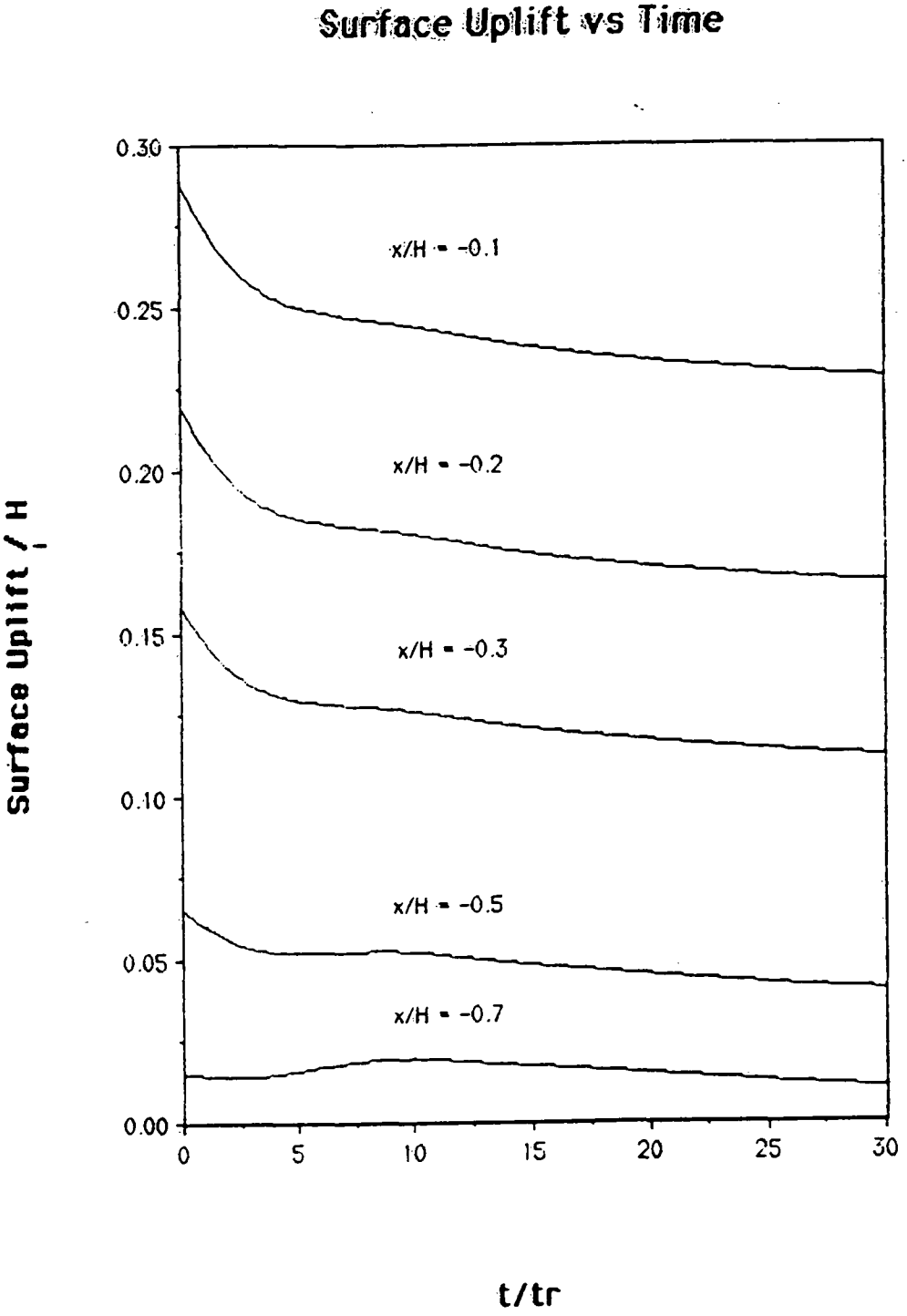
Surface Uplift vs Time
Surface Uplift / H
0.30
0.25
0.20
0.15
0.10
0.05
0.00
x/H = -0.1
x/H = -0.2
x/H = -0.3
x/H = -0.5
x/H = -0.7
0
5
10
15
20
25
30
t/tr

Figure 7

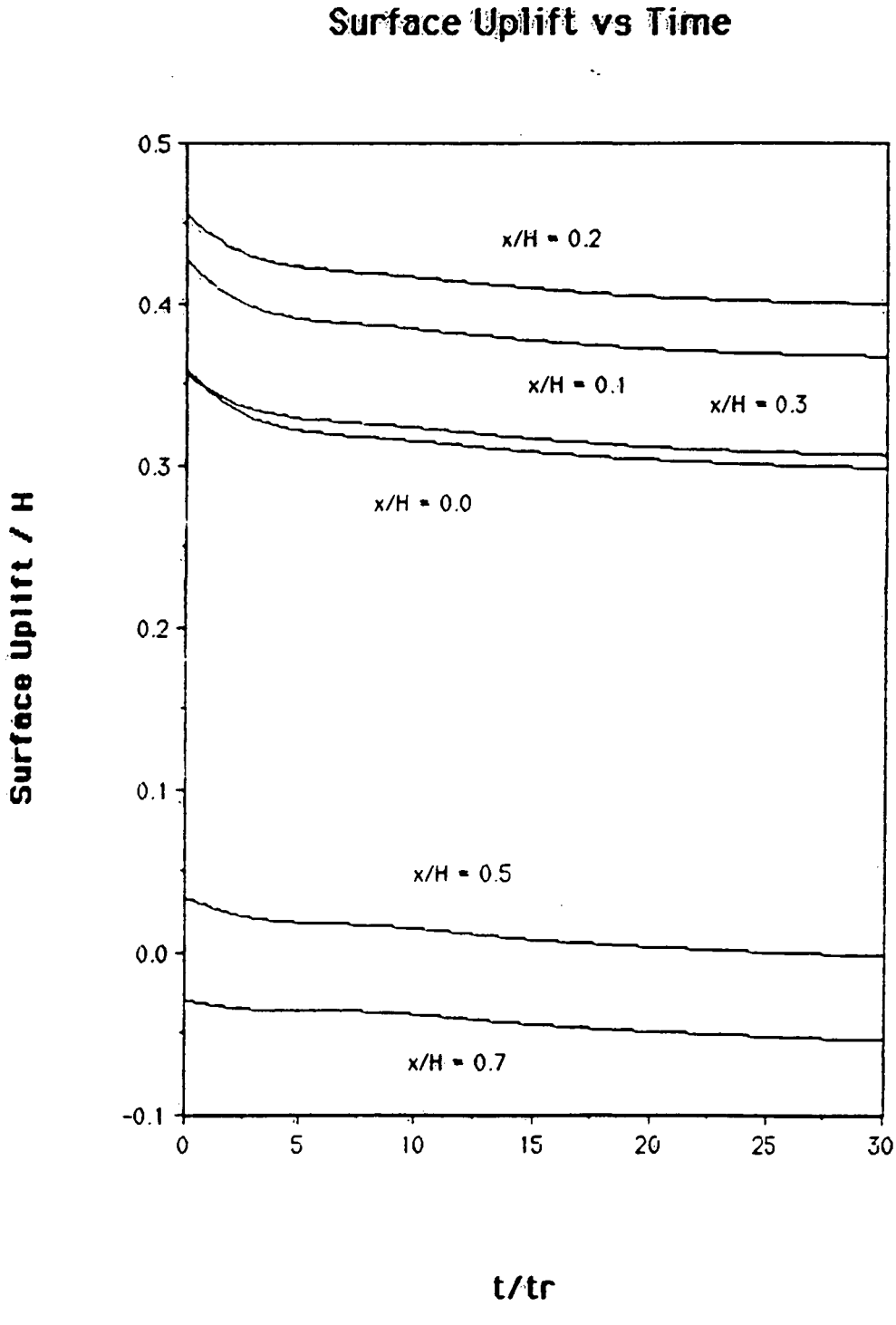
Surface Uplift vs Time
Surface Uplift / H
0.5
0.4
0.3
0.2
0.1
0.0
-0.1
0
5
10
15
20
25
30
t/tr
x/H = 0.2
x/H = 0.1
x/H = 0.3
x/H = 0.0
x/H = 0.5
x/H = 0.7

Figure 8

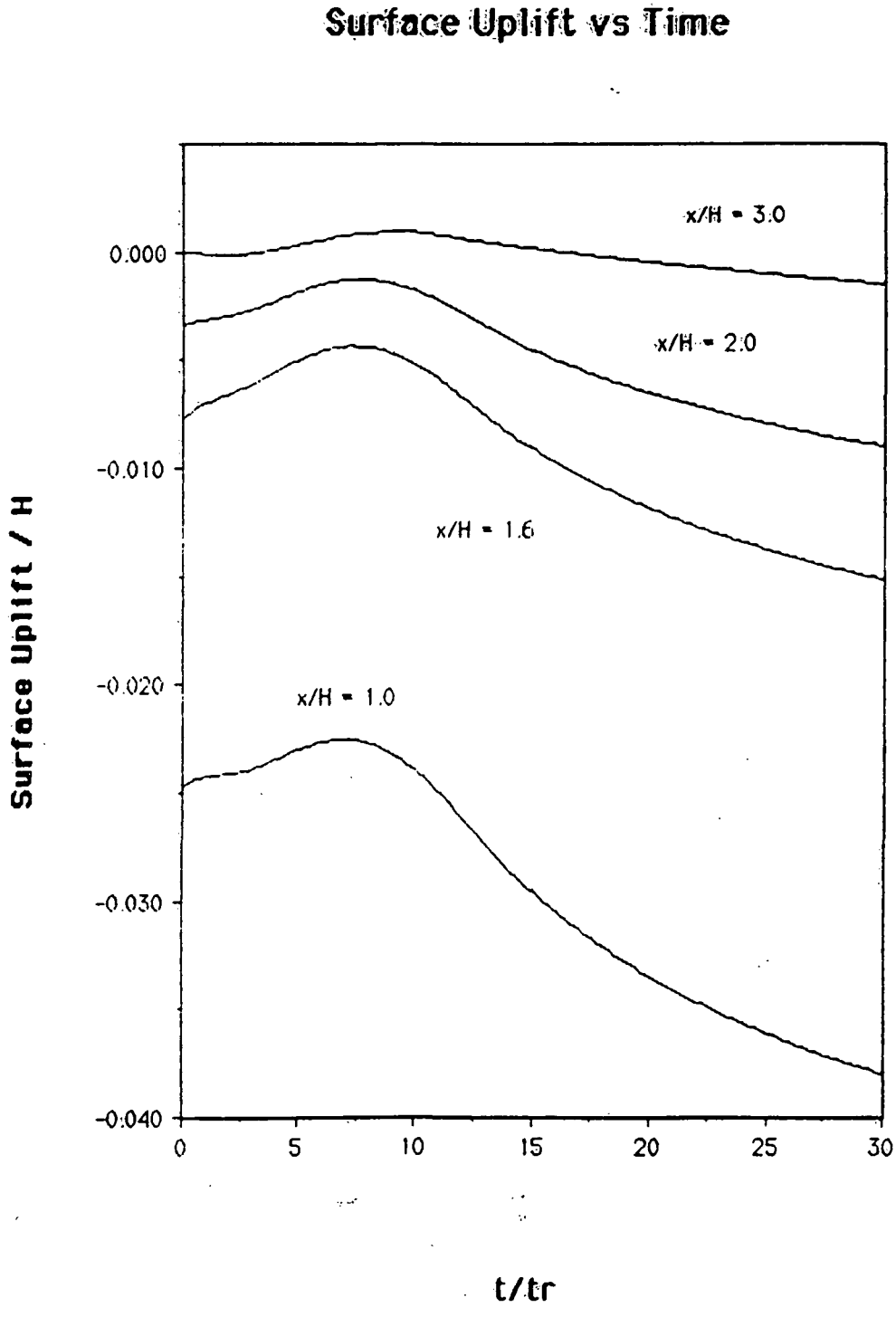
Surface Uplift vs Time
x/H = 3.0
x/H = 2.0
x/H = 1.6
x/H = 1.0
0.000
-0.010
-0.020
-0.030
-0.040
0
5
10
15
20
25
30
Surface Uplift / H
t/tr

Figure 9

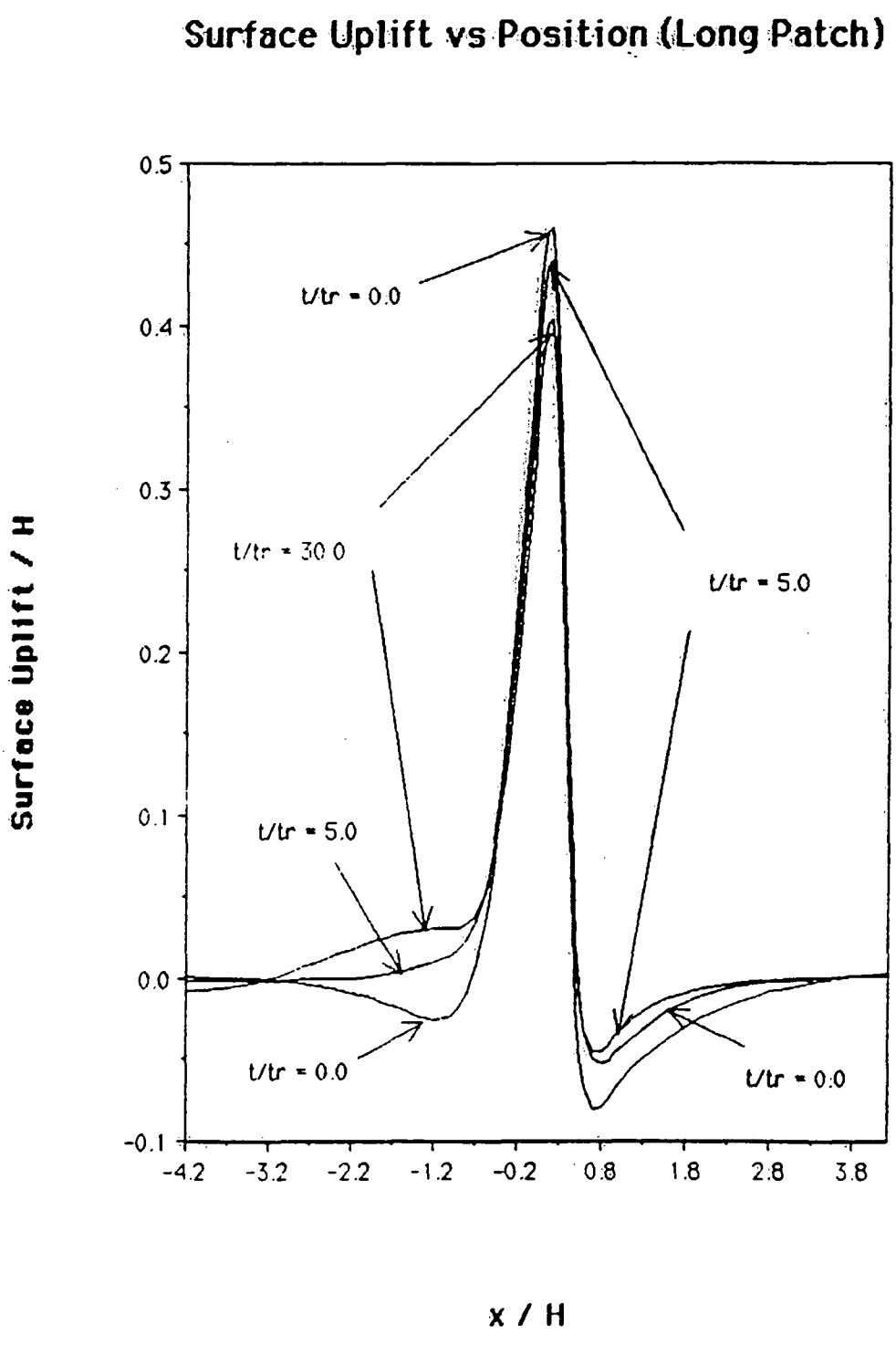
Surface Uplift vs Position (Long Patch)
Surface Uplift / H
x / H
0.5
0.4
0.3
0.2
0.1
0.0
-0.1
-4.2
-3.2
-2.2
-1.2
-0.2
0.8
1.8
2.8
3.8
t/tr = 0.0
t/tr = 30.0
t/tr = 5.0
t/tr = 5.0
t/tr = 0.0
t/tr = 0.0

Figure 10

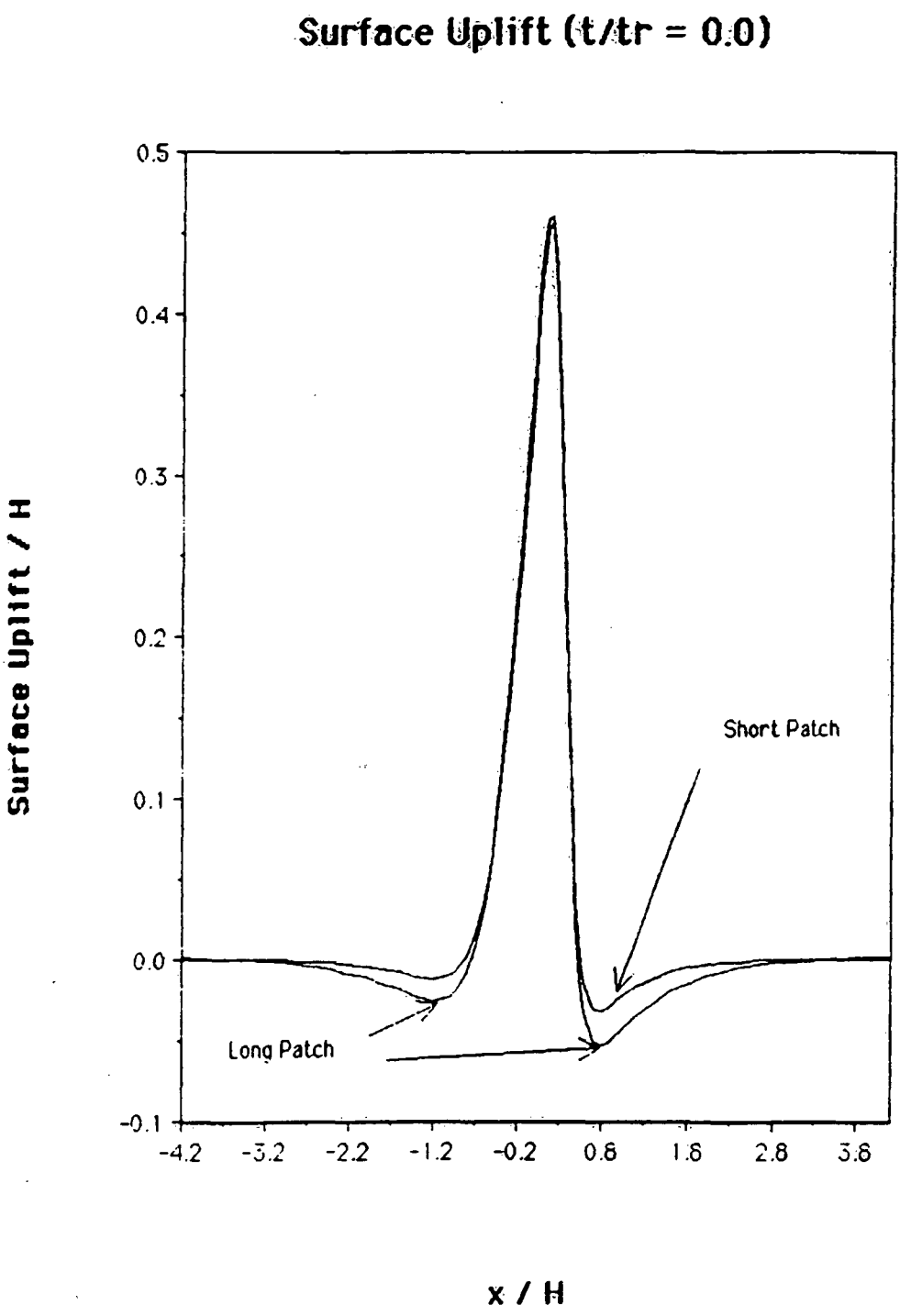
Surface Uplift (t/tr = 0.0)
Surface Uplift / H
0.5
0.4
0.3
0.2
0.1
0.0
-0.1
-4.2
-3.2
-2.2
-1.2
-0.2
0.8
1.8
2.8
3.8
Short Patch
Long Patch
x / H

Figure 11

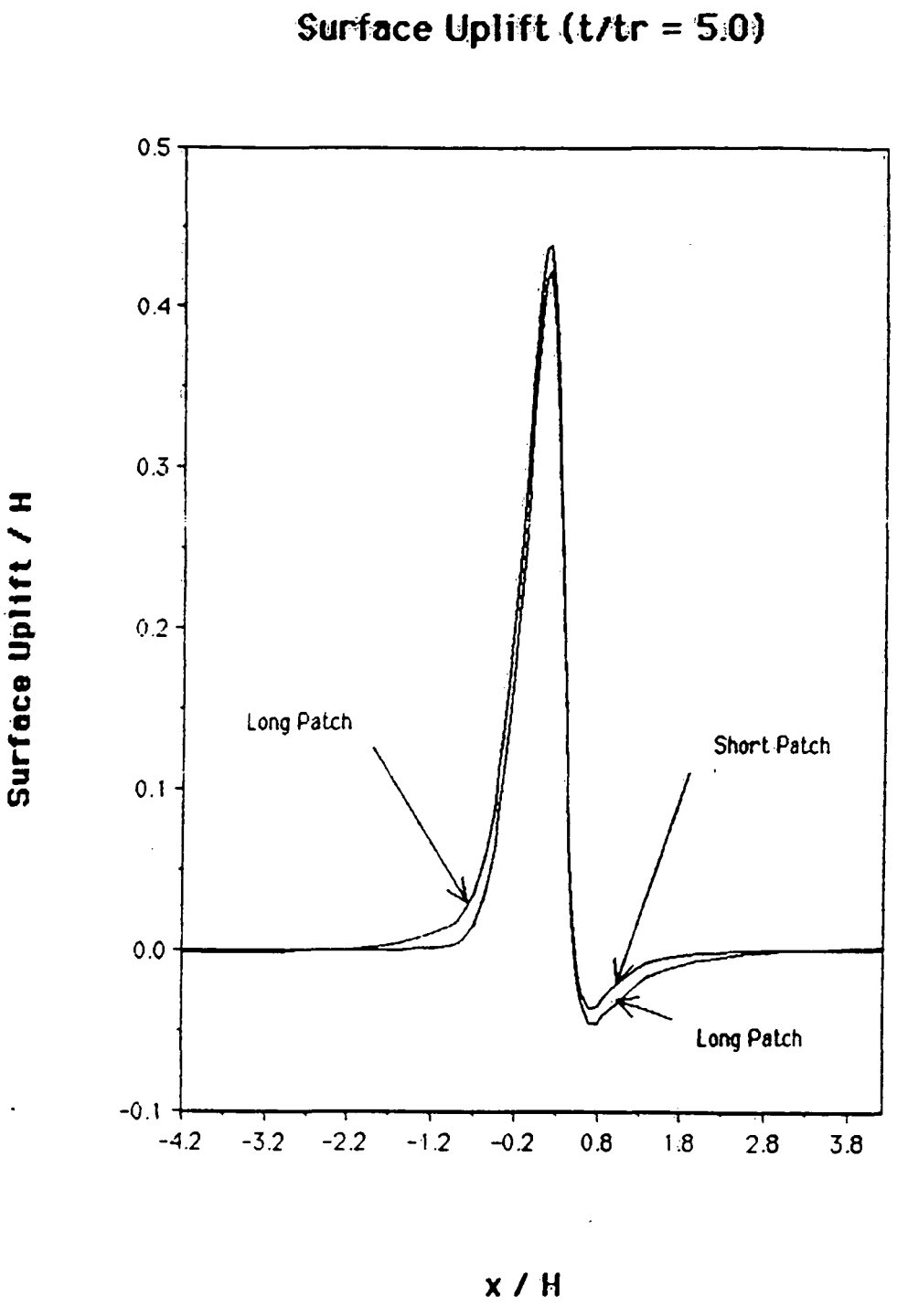
Surface Uplift (t/tr = 5.0)
Surface Uplift / H
0.5
0.4
0.3
0.2
0.1
0.0
-0.1
-4.2
-3.2
-2.2
-1.2
-0.2
0.8
1.8
2.8
3.8
Long Patch
Short Patch
Long Patch
x / H

Figure 12

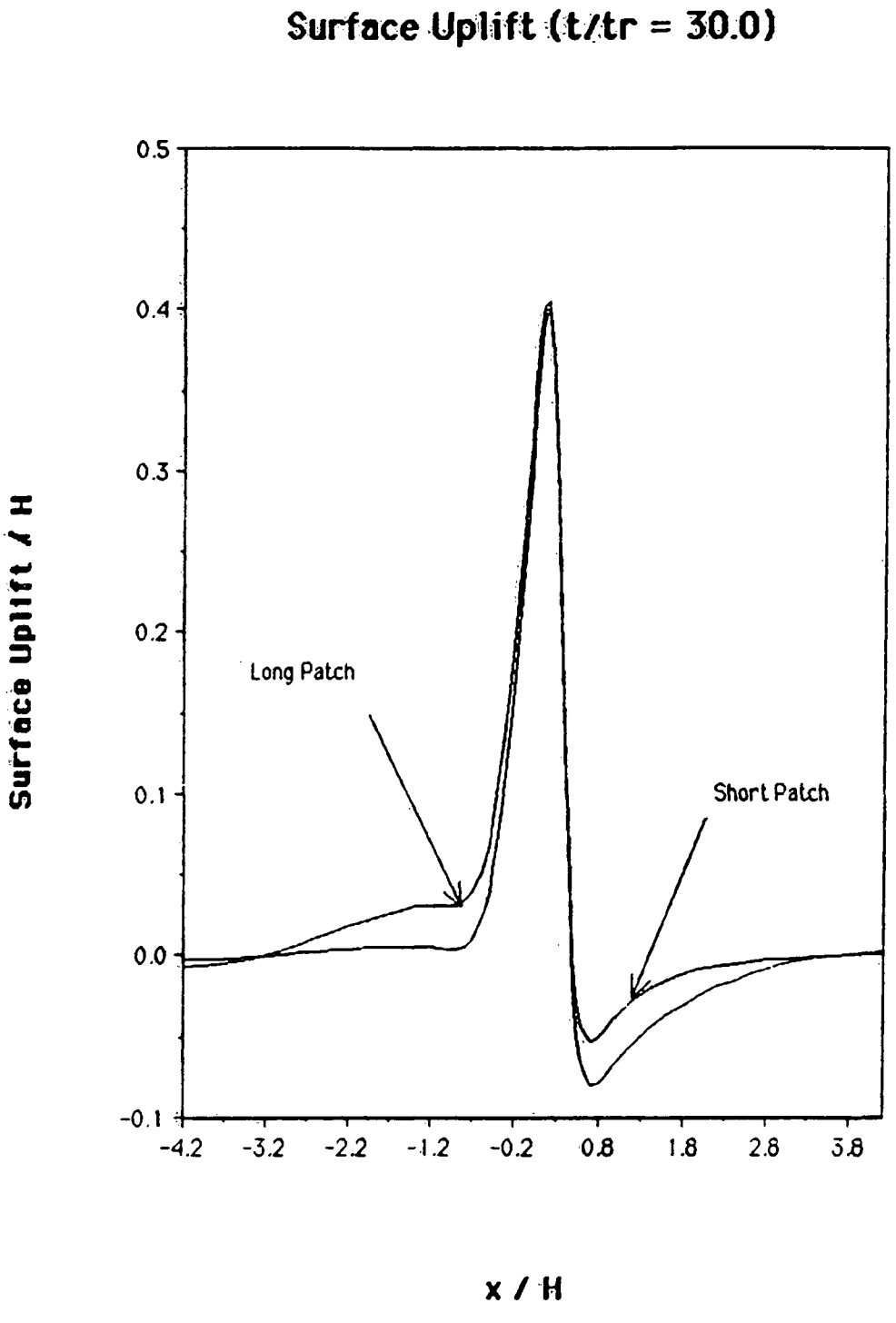
Surface Uplift (t/tr = 30.0)
Surface Uplift / H
0.5
0.4
0.3
0.2
0.1
0.0
-0.1
Long Patch
Short Patch
-4.2
-3.2
-2.2
-1.2
-0.2
0.8
1.8
2.8
3.8
x / H

Figure 13